Chinese Chemical Letters 35 (2024) 108521

Contents lists available at ScienceDirect

Chinese Chemical Letters

journal homepage: www.elsevier.com/locate/cclet

Incorporation sodium ions into monodisperse lead-free double perovskite $Cs_2AgBiCl_6$ nanocrystals to improve optical properties

Song Wang[a], Ying Xie[a], Wenchao Jiang[c], Binghang Liu[a], Keying Shi[a,*], Kai Pan[a,b,*]

[a] Key Laboratory of Functional Inorganic Material Chemistry, Ministry of Education, Heilongjiang University, Harbin 150080, China
[b] School of Materials Science and Engineering, Jiangsu Engineering Laboratory of Light-Electricity-Heat Energy-Converting Materials and Applications, Changzhou University, Changzhou 213164, China
[c] State Key Laboratory of Catalysis, Dalian National Laboratory for Clean Energy, Dalian Institute of Chemical Physics, Chinese Academy of Sciences, Dalian 116023, China

ARTICLE INFO

Article history:
Received 10 January 2023
Revised 18 March 2023
Accepted 26 April 2023
Available online 30 April 2023

Keywords:
Nanocrystals
Alloy
Double perovskites
Optical properties
Exciton binding energy

ABSTRACT

Lead-free double perovskite nanocrystals (NCs) have emerged as a promising candidate in the optical field, owing to their non-toxic, good moist heat and chemical stability. However, their poor optical properties limited their application. To improve the optical properties of lead-free double perovskite NCs, metal ion doping or alloying had been suggested as a promising strategy. Here, we prepared monodisperse, uniformly sized, cubic morphology of $Cs_2AgBiCl_6$ NCs with different Na^+ incorporation amounts *via* a simple hot-injection method. The Na^+ incorporation broke the parity-forbidden transition by reducing the inversion symmetry of the electron wave function at the Ag site, which changed the parity of the self-trapped exciton wave function and thus allowed radiative recombination. As a result, the photoluminescence quantum yield (PLQY) of Na^+-alloyed $Cs_2AgBiCl_6$ NCs (12.1%) was higher than that of $Cs_2AgBiCl_6$ NCs (2.4%), and the exciton lifetime of Na^+-alloyed $Cs_2AgBiCl_6$ NCs increased to 36.98 ns from 17.58 ns for $Cs_2AgBiCl_6$ NCs. By adjusting the amount of Na^+ incorporation, the band gap of $Cs_2AgBiCl_6$ NCs can be significantly tuned from ~2.90 eV to ~3.50 eV. Furthermore, the temperature-dependent photoluminescence spectra indicated that the Na^+-alloyed $Cs_2AgBiCl_6$ NCs possessed higher longitudinal optical phonon energy and exciton binding energy compared to $Cs_2AgBiCl_6$ NCs. This suggested that there were strong exciton-phonon interactions during exciton recombination, a reduced probability of non-radiative processes, and excellent thermal stability. It offers a promising strategy for improving the optical properties of lead-free double perovskite NCs, and have the potential to replace traditional lead halide perovskite NCs in future optoelectronic applications.

Lead halide perovskite nanocrystals (NCs) possess a unique three-dimensional perovskite structure and exhibit excellent carrier behavior, resulting in outstanding optical properties [1–4]. As a result, these NCs have found widespread use in optoelectronic applications such as light-emitting diodes [4–8], lasers [9–11], solar cells [12–16], non-linear optics [17], and photodetectors [18,19]. However, their toxicity, poor moist heat, and chemical stability severely limit their potential for further applications [20–23]. Therefore, there is an urgent need to explore lead-free perovskite NCs that offer comparable electronic, structural, and optical properties to those of lead halide perovskite NCs.

Lead halide perovskite NCs can be modified by replacing two Pb^{2+} ions with one monovalent (M^+) and one trivalent (M^{3+}) metal ion to form $Cs_2M^+M^{3+}X_6$ double perovskite NCs ($M^+ = Na^+$, Ag^+, *etc.*, $M^{3+} = In^{3+}$, Bi^{3+}, Sb^{3+}, *etc.*, X = Cl, Br, I). This strategy has been proven to effectively reduce toxicity and increase the stability of the NCs [24–31]. However, these double perovskite NCs have weaker photoluminescence (PL) and lower photoluminescence quantum yield (PLQY) compared to conventional lead halide perovskite NCs. This is due to their indirect band gaps or direct band gaps characterized by the parity forbidden transitions [26,29,32-34], despite having a similar three-dimensional perovskite structure and electrical neutrality.

Doping or alloying double perovskite NCs with metal ions is an effective way to improve their band gap structure or parity forbidden transition, leading to enhanced PL intensity and PLQY. For instance, Xia's group prepared $Cs_2AgInCl_6$ NCs and Bi^{3+}-doped $Cs_2AgInCl_6$ NCs using a simple hot-injection method [28]. Bi^{3+} doping adjusted the band gap of $Cs_2AgInCl_6$ NCs from 4.25 eV

* Corresponding authors.
E-mail addresses: shikeying2008@163.com (K. Shi), kaipan@hlju.edu.cn (K. Pan).

https://doi.org/10.1016/j.cclet.2023.108521
1001-8417/

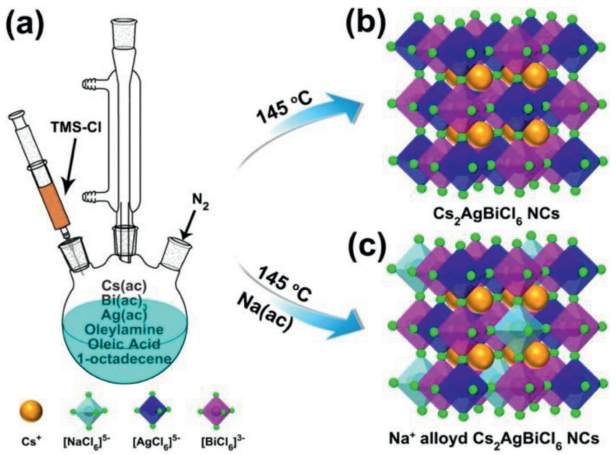

Fig. 1. (a) Colloidal synthesis of double perovskite $Cs_2AgBiCl_6$ NCs and Na^+-alloyed $Cs_2AgBiCl_6$ NCs. Crystal structure of (b) $Cs_2AgBiCl_6$ NCs and (c) Na^+-alloyed $Cs_2AgBiCl_6$ NCs.

to 3.28 eV, and altered the emission spectrum from blue to orange. Meanwhile, Bi^{3+} doping significantly improved the PLQY of $Cs_2AgInCl_6$ NCs (~11.4%). Han's group prepared $Cs_2NaInCl_6$ NCs and Ag^+-doped $Cs_2NaInCl_6$ NCs using a variable temperature hot-injection method [35]. Ag^+ doping transformed the dark self-trapping excitons (STEs) state of $Cs_2NaInCl_6$ NCs into a bright STEs state, which was attributed to the interaction between $[AgCl_6]^{5-}$ and $[NaCl_6]^{5-}$ octahedra breaking the parity forbidden transition, resulting in bright yellow emission. The PLQY of Ag^+-doped $Cs_2NaInCl_6$ NCs was significantly enhanced (~31.1%) compared to that of $Cs_2NaInCl_6$ NCs. Moreover, they also prepared Mn^{2+}-doped $Cs_2NaIn_xBi_{1-x}Cl_6$ ($0 < x < 1$) NCs using a colloidal synthesis strategy [36]. The emission spectrum changed from blue emission to bright orange-red emission. Meanwhile, the PLQY of Mn^{2+}-doped $Cs_2NaIn_xBi_{1-x}Cl_6$ ($0 < x < 1$) NCs can reach 44.6% compared to the undoped NCs (~38%). However, there were relatively fewer reports on alkali metal-alloyed double perovskite NCs, and the effect of such incorporation on the exciton binding energy and longitudinal optical phonons of double perovskite NCs remains unexplored.

In this work, we prepared a series of monodisperse, uniformly sized cube morphology $Cs_2AgBiCl_6$ NCs with different Na^+ incorporation amounts *via* a simple hot-injection method. By varying the amount of Na^+ incorporation, we were able to significantly tune the band gap of the $Cs_2AgBiCl_6$ NCs from ~2.90 eV to ~3.50 eV. The 56% Na^+-alloyed $Cs_2AgBiCl_6$ NCs exhibited the strongest PL and the highest PLQY (12.1%) compared to other NCs, and the exciton lifetime was also extended from 17.58 ns to 36.98 ns. It was noteworthy that the 56% Na^+-alloyed $Cs_2AgBiCl_6$ NCs exhibited higher exciton binding energy and longitudinal optical phonon energy than $Cs_2AgBiCl_6$ NCs. This indicated 56% Na^+-alloyed $Cs_2AgBiCl_6$ NCs possessed excellent thermal stability, strong exciton-phonon interactions, and lower non-radiative probability. Our findings highlight the crucial role of metal ion incorporation in regulating the band gap and optical properties of double perovskite NCs.

$Cs_2AgBiCl_6$ NCs with different Na^+ incorporation amounts were prepared *via* a simple hot-injection method (Fig. 1a). Briefly, Cs(ac), $Bi(ac)_3$, Ag(ac)/Na(ac) were dissolved in a mixed solution of ODE, OA, and OAm. The mixed solution was heated until the temperature reached 145 °C, followed by the rapid injection of trimethylchlorosilane (TMS-Cl) to initiate nucleation and crystallization of the NCs (see the experimental section in Supporting information for details). $Cs_2AgBiCl_6$ NCs with different Na^+ incorporation amounts was obtained by adjusting the ratio of Ag/Na metal precursors (Table S1 in Supporting information). The precise Na^+ incorporation amounts of $Cs_2AgBiCl_6$ NCs were obtained by inductively coupled plasma optical emission spectrometer (ICP-OES), which were 8%, 26%, 56% and 74%, respectively (Table S2 in Supporting information). In addition, the crystal structure diagrams of $Cs_2AgBiCl_6$ NCs and Na^+-alloyed $Cs_2AgBiCl_6$ NCs were shown in Figs. 1b and c.

The X-ray diffraction patterns (XRD) of $Cs_2AgBiCl_6$ NCs with different Na^+ amounts were shown in Fig. S1a (Supporting information). The XRD results revealed that $Cs_2AgBiCl_6$ NCs with different Na^+ incorporation amounts possessed a cubic double perovskite structure with Fm-3m space group [32]. The sharp diffraction peaks of the NCs indicated good crystallinity. Furthermore, as the Na^+ incorporation amounts increased, the XRD diffraction peaks of Na^+-alloyed $Cs_2AgBiCl_6$ NCs were shifted towards a smaller 2θ angle, which was attributed to the bond length of the newly formed Na-Cl bond (2.736 Å) [37] was longer than that of the Ag-Cl bond (2.708 Å) [38], resulted in lattice expansion. Fig. S1b (Supporting information) provided a magnified view of the (220) diffraction peak, further confirming the shift of the diffraction peak to smaller 2θ angles. With the increase of Na^+ incorporation amount, the intensity of the (111) crystal plane diffraction peak gradually increases (marked with an asterisk in Fig. S1a), which was related to the difference in scattering factors of Na and Ag atoms, indicating that alloyed $Cs_2Ag_{1-x}Na_xBiCl_6$ NCs would be formed when working under the intermediate composition of Na/Ag [39].

The UV-vis absorption spectra of $Cs_2AgBiCl_6$ NCs with different Na^+ incorporation amounts were shown in Fig. S1c (Supporting information). The exciton absorption peak was observed to blue shift from 364 nm to 326 nm with an increase in Na^+ incorporation amount. This corresponds to a change in exciton absorption energy from 3.40 eV to 3.80 eV (Fig. S1d in Supporting information) and an increase in PLQY from 2.4% to 12.1% (Table S3 in Supporting information). In order to display the measurement results, we added distribution histograms of the PLQY results as Fig. S2 (Supporting information). Each measurement result was either close to or equal to the average value, indicating that our results exhibited a good repeatability. Meanwhile, the band gap values of Na^+-alloyed $Cs_2AgBiCl_6$ NCs were estimated according to the Tauc plots (Fig. S3 in Supporting information), revealing an increase in band gap from 2.9 eV to 3.5 eV with an increase in Na^+ incorporation amount (Fig. S1d). This could be attributed to the participation of Na^+ orbitals (Na-s) in the formation of the conduction band minimum (CBM) of Na^+-alloyed $Cs_2AgBiCl_6$ NCs, which regulates the electronic structure of the NCs [40,41].

PL spectra showed that Na^+ incorporation into the $Cs_2AgBiCl_6$ NCs produced a broad emission peak centered at 615 nm (Fig. S1e in Supporting information), which was attributed to the STEs state [39]. With the increase of Na^+ incorporation amounts, the intensity of the broad emission peak increases gradually, indicating more free excitons were transferred to the STEs state to form self-trapped domain excitons. There were two reasons for the difference in PLQY with different doping gradient. Firstly, Na doping broke the inversion-symmetry-induced parity-forbidden transition of the $Cs_2AgBiCl_6$ NCs lattice by reducing the inversion symmetry of the electron wave function at the Ag site, which changed the parity of the STEs wave function and allowed radiative recombination. Secondly, the $[NaCl_6]^{5-}$ octahedra could act as barriers to restrict the spatial distribution of STEs. The incorporation amount increased from 26% to 56%, with a large doping gradient, resulting in a significant increased orbitals overlap and the transition dipole moment [42,43]. Therefore, the PLQY increased from 7.6% to 12.1%. Interestingly, the 56% Na^+-alloyed $Cs_2AgBiCl_6$ NCs possessed the strongest emission peak and the largest PLQY value (~12.1%) compared to other Na^+-alloyed $Cs_2AgBiCl_6$ NCs (Table S3). However, the intensity of the emission peak decreased with the increase of Na^+ incorporation amounts, which might be caused by the concen-

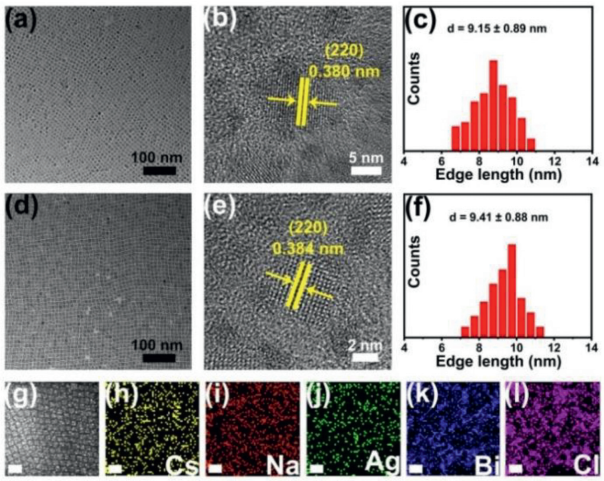

Fig. 2. Transmission electron microscopy (TEM) images of (a) $Cs_2AgBiCl_6$ NCs and (d) 56% Na^+-alloyed $Cs_2AgBiCl_6$ NCs. High-resolution TEM (HRTEM) images of (b) $Cs_2AgBiCl_6$ NCs and (e) 56% Na^+-alloyed $Cs_2AgBiCl_6$ NCs. Edge length distribution histogram of (c) $Cs_2AgBiCl_6$ NCs and (f) 56% Na^+-alloyed $Cs_2AgBiCl_6$ NCs. High-angle annular dark field scanning transmission electron microscopy (HAADF-STEM) image of (g) 56% Na^+-alloyed $Cs_2AgBiCl_6$ NCs and corresponding elemental mapping images of (h) Cs, (i) Na, (j) Ag, (k) Bi, and (l) Cl, respectively. Scale bars are 20 nm.

tration quenching effect [44,45]. In addition, $Cs_2NaBiCl_6$ NCs did not had a broad emission peak, which was mainly due to the existence of dark STEs state (Fig. S1f in Supporting information) [46].

Transmission electron microscopy (TEM) images (Figs. 2a and c, Fig. S4 in Supporting information) and the histograms of the edge length distribution (Figs. 2e and f, Fig. S4) demonstrated the microscopic morphology and edge length distribution of $Cs_2AgBiCl_6$ NCs with different Na^+ incorporation amounts, respectively. The $Cs_2AgBiCl_6$ NCs with different Na^+ incorporation amounts exhibited uniform, monodisperse cubic morphology. The edge length of the Na^+-alloyed $Cs_2AgBiCl_6$ NCs gradually increased from 9.15 ± 0.89 nm to 9.63 ± 0.86 nm with increased Na^+ incorporation amounts (Fig. S5 in Supporting information). This was attributed to the larger lattice constant of $Cs_2NaBiCl_6$ NCs (10.84 Å) compared to that of $Cs_2AgBiCl_6$ NCs (10.78 Å). The 56% Na^+-alloyed $Cs_2AgBiCl_6$ NCs were further investigated due to their highest PLQY (12.1%). High-resolution TEM (HRTEM) images of $Cs_2AgBiCl_6$ NCs and 56% Na^+-alloyed $Cs_2AgBiCl_6$ showed that both NCs had clear, highly crystalline lattice fringes and exhibited a cubic crystal structure corresponding to the (220) crystal plane (Figs. 2b and d). The lattice constant of the 56% Na^+-alloyed $Cs_2AgBiCl_6$ NCs was found to have increased slightly from 0.380 nm ($Cs_2AgBiCl_6$ NCs) to 0.384 nm. This could be attributed to the formation of a longer Na-Cl bond, compared to the Ag-Cl bond, which resulted in lattice expansion, which was consistent with the XRD results discussed earlier. The high-angle annular dark field scanning transmission electron microscopy (HAADF-STEM) and energy dispersive X-ray spectroscopy (EDS) elemental mapping of 56% Na^+-alloyed $Cs_2AgBiCl_6$ NCs were shown in Figs. 2g-l. The presence and homogeneous distribution of Cs, Na, Ag, Bi and Cl elements in the 56% Na^+-alloyed $Cs_2AgBiCl_6$ NCs confirmed the successful incorporation of Na^+ into the $Cs_2AgBiCl_6$ NCs.

In order to further confirm the existence of Na^+, the $Cs_2AgBiCl_6$ NCs and 56% Na^+-alloyed $Cs_2AgBiCl_6$ NCs were tested by X-ray photoelectron spectroscopy (XPS) [47]. Compared with $Cs_2AgBiCl_6$ NCs, an additional clear Na 1s peak appeared on the full XPS spectrum of 56% Na^+-alloyed $Cs_2AgBiCl_6$ NCs (Fig. S6a in Supporting information), meanwhile, in the high-resolution XPS spectrum of Na 1s (Fig. S6b in Supporting information), a Na 1s peak was displayed at 1070.7 eV, which confirmed the successful incorporation

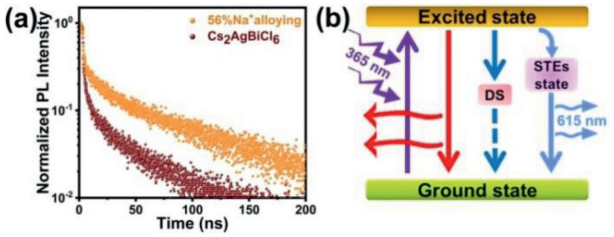

Fig. 3. (a) Time-resolved PL (TRPL) decay profiles of $Cs_2AgBiCl_6$ NCs (wine) and 56% Na^+-alloyed $Cs_2AgBiCl_6$ NCs (orange). (b) The PL mechanism of Na^+-alloyed $Cs_2AgBiCl_6$ (DS: defect state; STEs: self-trapped excitons).

of Na^+ into the $Cs_2AgBiCl_6$ NCs. The high-resolution XPS spectra of Cs 3d, Ag 3d, Bi 4f, and Cl 2p were shown in Figs. S6c-f (Supporting information). When compared to $Cs_2AgBiCl_6$ NCs, the binding energy peaks of Ag 3d and Cl 2p of 56% Na^+-alloyed $Cs_2AgBiCl_6$ NCs were shifted towards lower binding energy (Figs. S6d and f), suggesting that the incorporation of Na^+ weakens the Ag-Cl bond. This was attributed to the lower electronegativity of Na relative to Ag, which resulted in a stronger Na-Cl bond [48,49]. Moreover, the peaks of binding energy for Cs 3d and Bi 4f were slightly shifted towards the lower binding energy (Figs. S6c and e). This was attributed to the increased electron density of Cl around Cs and the weakened interaction between Bi and Cl [50].

Fig. 3a showed the time-resolved PL (TRPL) decay curves of $Cs_2AgBiCl_6$ NCs and 56% Na^+-alloyed $Cs_2AgBiCl_6$ NCs. The TRPL decay curve was fitted with a double exponential decay [51], and the luminescence lifetime decay time (τ_i) and relative amplitude (A_i) were obtained, which was summarized in Table S4 (Supporting information). According to formula $\tau_{avg} = \sum_i^n (A_i\tau_i^2/A_i\tau_i)$, the average decay times of $Cs_2AgBiCl_6$ NCs and 56% Na^+-alloyed $Cs_2AgBiCl_6$ NCs were calculated to be 17.58 ns and 36.98 ns, respectively. This indicated that the incorporation of Na^+ can effectively enhance the exciton lifetime of $Cs_2AgBiCl_6$ NCs and prolonged the exciton lifetime by about 2.1 times, which could be attributed to the formation of STEs state resulting from the incorporation of Na^+ [39]. Based on the results discussed above, a possible PL mechanism of Na^+-alloyed $Cs_2AgBiCl_6$ NCs was proposed (Fig. 3b). Under the light excitation of 365 nm, the carriers were excited from the ground state to the excited state, which led to the formation free excitons locally. These free excitons undergo non-radiative relaxation and transferred to the STEs state, resulting in the formation of STEs. Finally, the recombination of STEs generated a broad emission peak.

To investigate the impact of Na^+ incorporation on the PL properties of $Cs_2AgBiCl_6$ NCs, we obtained temperature-dependent PL spectra of both the $Cs_2AgBiCl_6$ NCs and 56% Na^+-alloyed $Cs_2AgBiCl_6$ NCs within the range of 80-300 K. These spectra were showed in Figs. 4a-d. The temperature-dependent PL spectra provided insight into the exciton binding energy (E_b) and the exciton-phonon interaction of the NCs. As shown in Figs. 4a and b, the PL intensities of both NCs decrease with increasing temperature, which was attributed to the creation of more non-radiative decay channels with increasing temperature [52]. The variation of PL intensity with temperature (Fig. 4e) was fitted according to Eq. 1 [7,53].

$$I(\mathrm{T}) = \frac{I_0}{1 + Ae^{-E_b/k_bT}} \quad (1)$$

where $I(T)$ and I_0 are the integrated PL intensity at temperature T and 0 K, respectively, E_b is the exciton binding energy, and k_b is the Boltzmann constant. The fitting results in Fig. 4e revealed that the E_b for $Cs_2AgBiCl_6$ NCs and 56% Na^+-alloyed $Cs_2AgBiCl_6$ NCs were 170 meV and 223 meV, respectively. The significant increase in E_b for 56% Na^+-alloyed $Cs_2AgBiCl_6$ NCs suggested a higher probabil-

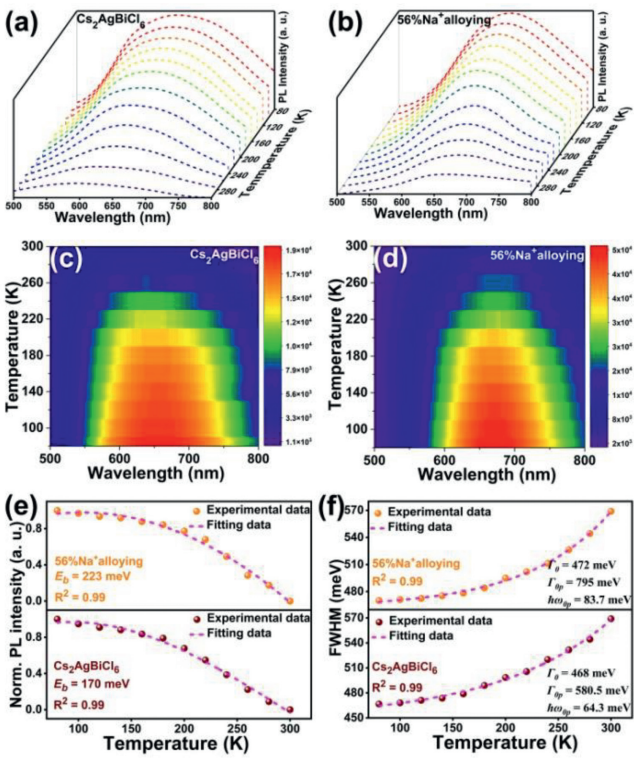

Fig. 4. (a) Waterfall maps of temperature-dependent PL spectra of (a) $Cs_2AgBiCl_6$ NCs and (b) 56% Na^+-alloyed $Cs_2AgBiCl_6$ NCs. The 2D color maps of temperature-dependent PL spectra of (c) $Cs_2AgBiCl_6$ NCs and (d) 56% Na^+-alloyed $Cs_2AgBiCl_6$ NCs. (e) Integrated PL intensity and (f) FWHM as a function of temperature.

ity of radiative recombination compared to $Cs_2AgBiCl_6$ NCs [54]. Moreover, this result indicates that 56% Na^+-alloyed $Cs_2AgBiCl_6$ NCs exhibited relatively high thermal stability [55]. However, the PLQY of 56% Na^+-alloyed $Cs_2AgBiCl_6$ NCs was relatively low compared to other reported double perovskites [35,42]. This was attributed to the fact that 56% Na^+-alloyed $Cs_2AgBiCl_6$ NCs were an indirect band gap material. Meanwhile, the colloidal synthesis led to the production of surface defects, which further decreased the PLQY.

Meanwhile, the interaction between excitons and phonons during carrier recombination was studied by analyzing the broadening behavior of the full-width half-maximum (FWHM) of the PL peak. Fig. 4f showed the variation of FWHM with temperature for $Cs_2AgBiCl_6$ NCs and 56% Na^+-alloyed $Cs_2AgBiCl_6$ NCs. The variation of FWHM with temperature was fitted according to Eq. 2 [56,57].

$$\Gamma(T) = \Gamma_0 + \frac{\Gamma_{0p}}{e^{\hbar\omega_{0p}/k_bT} - 1} \quad (2)$$

where $\Gamma(T)$ is the FWHM of the sample at temperature T, Γ_0 is the inhomogeneous broadening contribution at 0 K, Γ_{op} is the exciton-optical phonon coefficient, $\hbar\omega_{op}$ is the longitudinal optical phonon energy, and k_b is the Boltzmann constant. Based on the fitting results in Fig. 4f, we determined that the $\hbar\omega_{op}$ values for $Cs_2AgBiCl_6$ NCs and 56% Na^+-alloyed $Cs_2AgBiCl_6$ NCs were 64.3 meV and 83.7 meV, respectively. The $Cs_2AgBiCl_6$ NCs exhibited a smaller $\hbar\omega_{op}$ value, indicating that more phonons were generated and become non-radiative recombination centers. In contrast, 56% Na^+-alloyed $Cs_2AgBiCl_6$ NCs had a larger $\hbar\omega_{op}$ value, which suggested strong exciton-phonon interactions and lower non-radiative probability during exciton recombination [55].

In this work, we successfully prepared monodisperse, uniformly sized, cubic morphology of $Cs_2AgBiCl_6$ NCs with different Na^+ incorporation amounts *via* a simple hot-injection method. The incorporation of Na^+ directly affects the electronic structure and optical properties of $Cs_2AgBiCl_6$ NCs. By varying the amount of Na^+ incorporation, the band gap of the NCs was significantly tuned from ~2.90 eV to ~3.50 eV. Meanwhile, the 56% Na^+-alloyed $Cs_2AgBiCl_6$ NCs had the stronger PL and the higher PLQY (~12.1%) compared to the $Cs_2AgBiCl_6$ NCs (~2.4%), and the exciton lifetime was also extended ~2.1 times than $Cs_2AgBiCl_6$ NCs. Furthermore, temperature-dependent PL spectroscopy studies revealed that the 56% Na^+-alloyed $Cs_2AgBiCl_6$ NCs exhibited higher longitudinal optical phonon energy and exciton binding energy compared to the $Cs_2AgBiCl_6$ NCs, indicating their strong exciton-phonon interactions during exciton recombination, lower non-radiative probability, and good thermal stability. Overall, this study offers an effective approach for enhancing the optical properties of lead-free double perovskite NCs, which further advanced the potential application of their in the field of optoelectronics.

Declaration of competing interest

The authors declare that they have no known competing financial interests or personal relationships that could have appeared to influence the work reported in this paper.

Acknowledgments

We gratefully acknowledge the support of the National Natural Science Foundation of China (No. 21473051), the Natural Science Foundation of Heilongjiang Province (No. LH2019B014) and Youth Science and Technology Innovation Team Project of Heilongjiang Province (No. 2018-KYYWF-1593).

Supplementary materials

Supplementary material associated with this article can be found, in the online version, at doi:10.1016/j.cclet.2023.108521.

References

[1] G. Nedelcu, L. Protesescu, M.V. Kovalenko, et al., Nano Lett. 15 (2015) 5635–5640.
[2] Y.S. Park, S.J. Guo, V.I. Klimov, et al., ACS Nano 9 (2015) 10386–10393.
[3] L. Protesescu, S. Yakunin, M.V. Kovalenko, et al., Nano Lett. 15 (2015) 3692–3696.
[4] J.Z. Song, J.H. Li, H.B. Zeng, et al., Adv. Mater. 27 (2015) 7162–7167.
[5] Z.L. Gong, W. Zheng, X.U. Chen, et al., Angew. Chem. Int. Ed. 58 (2019) 6943–6947.
[6] D.B. Han, M. Imran, H.Z. Zhong, et al., ACS Nano 12 (2018) 8808–8816.
[7] X.M. Li, Y. Wu, H.B. Zeng, et al., Adv. Funct. Mater. 26 (2016) 2435–2445.
[8] C.Y. Wang, P. Liang, G.D. Wei, et al., Chem. Mater. 32 (2020) 7814–7821.
[9] L. Huang, Q.G. Gao, C.-H. Yan, et al., Adv. Mater. 30 (2018) 1800596.
[10] Y. Wang, X.M. Li, H.D. Sun, et al., Adv. Mater. 27 (2015) 7101–7108.
[11] H.M. Zhu, Y.P. Fu, X.Y. Zhu, et al., Nat. Mater. 14 (2015) 636–642.
[12] X.G. Yang, S.F. Zhang, D.H. Wang, et al., Chin. Chem. Lett. 33 (2022) 1425–1429.
[13] X.F. Ling, S.J Zhou, W.L. Ma, et al., Adv. Energy Mater. 9 (2019) 1900721.
[14] M.D. Que, Z.H. Dai, O. Chen, et al., ACS Energy Lett. 4 (2019) 1970–1975.
[15] Y. Zhang, O. Chen, Y.Y. Zhou, et al., Adv. Energy Mater. 9 (2019) 1900243.
[16] L. Chu, J.P. Yang, X.A. Li, et al., Nano-Micro Lett. 11 (2019) 16.
[17] Y. Wang, H.B. Zeng, H.D. Sun, et al., Nano Lett. 16 (2016) 448–453.
[18] T. Cai, W.W. Shi, O. Chen, et al., J. Am. Chem. Soc. 142 (2020) 11927–11936.
[19] W.L. Xu, M.S. Niu, X.T. Hao, et al., Chin. Chem. Lett. 32 (2021) 489–492.
[20] B. Hailegnaw, S. Kirmayer, D. Cahen, et al., J. Phys. Chem. Lett. 6 (2015) 1543–1547.
[21] K. Hills-Kimball, Y. Nagaoka, O. Chen, et al., J. Mater. Chem. C 5 (2017) 5680–5684.
[22] H. Huang, M.I. Bodnarchuk, A.L. Rogach, et al., ACS Energy Lett. 2 (2017) 2071–2083.
[23] Y. Nagaoka, K. Hills-Kimball, O. Chen, et al., Adv. Mater. 29 (2017) 1606666.
[24] N. Chen, T. Cai, O. Chen, et al., ACS Appl. Mater. Interfaces 11 (2019) 16855–16863.
[25] J.C. Dahl, W.T. Osowiecki, A.P. Alivisatos, et al., Chem. Mater. 31 (2019) 3134–3143.
[26] H.X. Yang, Y.B. Lou, Y.X. Zhao, et al., Chin. Chem. Lett. 33 (2022) 537–540.
[27] A. Karmakar, M.S. Dodd, V.K. Michaelis, et al., Chem. Mater. 30 (2018) 8280–8290.
[28] Y. Liu, Y. Jing, Z.G. Xia, et al., Chem. Mater. 31 (2019) 3333–3339.

[29] F. Locardi, M. Cirignano, L. Manna, et al., J. Am. Chem. Soc. 140 (2018) 12989–12995.
[30] Y.B. Yang, F. Hong, K.L. Han, et al., Angew. Chem. Int. Ed. 58 (2019) 2278–2283.
[31] B. Yang, X. Mao, K.L. Han, et al., J. Am. Chem. Soc. 140 (2018) 17001–17006.
[32] S.E. Creutz, E.N. Crites, D.R. Gamelin, et al., Nano Lett. 18 (2018) 1118–1123.
[33] J.J. Luo, S.R. Li, J. Tang, et al., ACS Photonics 5 (2018) 398–405.
[34] G. Volonakis, A.A. Haghighirad, F. Giustino, et al., J. Phys. Chem. Lett. 8 (2017) 772–778.
[35] P.G. Han, X. Mao, K.L. Han, et al., Angew. Chem. Int. Ed. 58 (2019) 17231–17235.
[36] P.G. Han, X. Zhang, K.L. Han, et al., ACS Cent. Sci. 6 (2020) 566–572.
[37] E.T. McClure, M.R. Ball, P.M. Woodward, et al., Chem. Mater. 28 (2016) 1348–1354.
[38] J.D. Majher, M.B. Gray, P.M. Woodward, et al., Chem. Mater. 31 (2019) 1738–1744.
[39] M.M. Yao, L. Wang, H.B. Yao, et al., Adv. Optical Mater. 8 (2020) 1901919.
[40] R.S. Lamba, P. Basera, S. Sapra, et al., J Phys. Chem. C 125 (2021) 1954–1962.
[41] J. Zhou, X.X. Rong, Z.G. Xia, et al., Adv. Optical Mater. 7 (2019) 1801435.
[42] J.J. Luo, E.H. Sargent, J. Tang, et al., Nature 563 (2018) 541–545.
[43] S. Li, Z.F. Shi, X.J. Li, et al., Chem. Mater. 31 (2019) 3917–3928.
[44] M. Shi, C. Li, R.G. Li, et al., Adv. Energy Mater. 2022 (2022) 1–11.
[45] Y. Liu, X.M. Rong, Z.G. Xia, et al., Angew. Chem. Int. Ed. 59 (2020) 11634–11640.
[46] D.X. Zhu, L. Manna, S. Brovelli, et al., ACS Energy Lett. 5 (2020) 1840–1847.
[47] Z.Y. Zhao, W. Xu, H.E. Song, et al., Mater. Res. Bull. 112 (2019) 142–146.
[48] D.W. Chen, X.G. Zhang, J.Z. Zhang, et al., Inorg. Chem. Front. 9 (2022) 4695–4704.
[49] C.J. Lu, J. Zhang, Y.J. Zhu, et al., Appl. Phys. Lett. 112 (2018) 193901.
[50] M. Shi, R.G. Li, C. Li, et al., Adv. Mater. 32 (2020) 2002137.
[51] Q.H. Liao, J.L. Chen, J.Z. Zhang, et al., J. Phys. Chem. Lett. 11 (2020) 8392–8398.
[52] Y.T. Liu, H.Z. Lu, L.R. Zheng, et al., AIP Adv. 8 (2018) 095108.
[53] X.W. Cheng, Z. Xie, X.Y. Chen, et al., Adv. Sci. 9 (2022) 2103724.
[54] M.Y. Leng, Y. Yang, J. Tang, et al., Nano Lett. 18 (2018) 6076–6083.
[55] R.R. Wu, Q. Wang, W.Z. Wu, et al., J. Alloy. Compd. 857 (2021) 157574.
[56] W.Z. Wu, W.L. Liu, Q.X. Yang, et al., J. Alloy. Compd. 787 (2019) 165–172.
[57] Q.J. Han, W.Z. Wu, Y.Q. Yang, et al., J. Lumin. 198 (2018) 350–356.